Exact solution for a photoacoustic wave from a finite-length cylindrical source

Jason Zalev
Seno Medical Instruments, 5253 Prue Road, Suite 315, San Antonio, Texas 78240

Michael C. Kolios[a)]
Department of Physics, Ryerson University, 350 Victoria Street, Toronto, Ontario M5B 2K3, Canada

(Received 15 May 2014; revised 26 January 2015; accepted 3 March 2015)

In wide-field pulsed photoacoustics, a nearly instantaneous source of electromagnetic energy is applied uniformly to an absorbing medium to create an acoustic wave. In this work, an exact solution is derived for the photoacoustic wave originating from a finite-length solid cylindrical source in terms of known analytic functions involving elliptic integrals of canonical form. The solution is compared with the output of a finite-element simulation.
 [http://dx.doi.org/10.1121/1.4916273]

[JDM] Pages: 1675–1682

I. INTRODUCTION

We derive an exact solution of the photoacoustic wave originating from a finite-length homogeneous solid circularly cylindrical source in terms of known analytic functions involving elliptic integrals of canonical form.

Our interest in this derivation originates in modeling photoacoustic waves produced from blood vessels in a vascular network. At near-infrared (NIR) optical wavelengths, blood is the strongest optical absorber in tissue.[1] A single blood vessel can be modeled as a finite-length solid cylinder. To model a full vascular network, the waves of many adjacent branching vessels can be added together in superposition. Our research deals with the geometrical arrangement of vessels in healthy and in abnormal biological tissues.[2,3] For instance, the vessels in healthy tissue are arranged in a highly organized manner, whereas in diseases like cancer, the vessels lose the ability to organize according to their usual branching patterns.[4] Hence, understanding photoacoustic waves produced by individual vascular segments and how the superposition of waves interact in three-dimensional (3D) vascular networks of different morphology is important in the monitoring, prevention, and treatment of disease.

It is known that no closed form solution exists in terms of basic mathematical functions[5] for the photoacoustic wave from a finite-length cylindrical source.[6,7] The solution to the problem is elliptic. The mathematical problem described in this paper was earlier studied by Remillard[6] for modeling the acoustic propagation of thunder caused by a columnar bolt of lightening in air. Remillard used numerical methods and an approximation of the solution for the finite-length cylindrical case was put forward involving a Rayleigh integral. Cylindrical geometries have historically been studied in photoacoustics[7–10] typically focusing on infinite-length geometry or numerical solutions of a Rayleigh integral. In other fields, finite-length cylinders may also be used to model submarines, airplanes, trees in a forest or microscopic structures such as bacteria and nanoparticles. In electromagnetics, finite-length cylinders can be used to model elements of a cylindrical wire antenna;[11–13] however, that problem is different from the photoacoustic problem because most of the current travels to the surface of the cylinder and the voltage potential is more akin to the acoustic velocity potential rather than the acoustic pressure. Acoustic radiation and scattering[14–17] have also been studied for finite-length cylinders, but the general problem also deals with modes of vibration and the problem usually involves an incident acoustic wave.

In this paper, the exact solution is reduced to terms that include elliptic integrals which can be computed efficiently and analyzed. Our implementation of computing the final form derived in this paper makes use of fast algorithms for evaluating elliptic integrals in canonical form. The mathematical form of the solution in terms of elliptic integrals may also permit construction of better and more accurate approximations for the exact solution.

Our approach is similar to Lamarche *et al.*[18] where the exact solution for the volume of intersection between a solid sphere and a solid infinite-length cylinder were reduced into terms of elliptic integrals for computing atomic cross-sections, where high precision was required. Lamarche *et al.* were able to transform his problem to a form that could be reduced to elliptic integrals. In our case, the surface area of intersection is used, rather than the volume of intersection, to represent a spherical acoustic wavefront. We also take additional steps to account for a finite-length that are possible when this approach is used.

To the best of our knowledge, the exact solution for a pressure wave resulting from a finite-length cylindrical source distribution has not elsewhere been solved in terms of known analytic functions.

II. PHOTOACOUSTIC WAVES

When a brief electromagnetic pulse illuminates a medium with a spatially distributed energy fluence $\Phi(\mathbf{x})$, the energy absorbed by the medium at position $\mathbf{x}$ is

[a)]Author to whom correspondence should be addressed. Electronic mail: mkolios@ryerson.ca

$$H(\mathbf{x}) = \mu_a(\mathbf{x})\Phi(\mathbf{x}), \tag{1}$$

where $\mu_a(\mathbf{x})$ is the absorption profile of the medium.

It is assumed that the pulse duration is short enough so that there will be *thermoelastic stress confinement*, where thermal conduction and stress propagation are negligible. Under this condition, a source of initial excess pressure will be created in the medium at $t = t_0 = 0$ according to

$$p_0(\mathbf{x}) = \frac{\beta(\mathbf{x})c^2(\mathbf{x})}{C_p(\mathbf{x})}H(\mathbf{x}), \tag{2}$$

where $\beta(\mathbf{x})$ is the thermal expansion coefficient, c is the speed of sound and $C_p(\mathbf{x})$ is the specific heat capacity. If the tissue is illuminated equally everywhere, such that $\Phi(\mathbf{x})$ is constant, this is called the *wide-field* photoacoustic assumption.

When the speed of sound in the medium is constant and the pulse is instantaneous, photoacoustic wave propagation is governed by the differential equation

$$\left(\frac{\partial^2}{\partial t^2} - c^2\nabla^2\right) p(\mathbf{x}, t) = p_0(\mathbf{x})\frac{\partial}{\partial t}\delta(t), \tag{3}$$

where $p(\mathbf{x}, t)$ is pressure and $\delta(t)$ is the Dirac impulse function.

Solving Eq. (3) under basic assumptions yields the forward solution for $p(\mathbf{x}, t)$ so that pressure at any time and position is[1,19,20]

$$p(\mathbf{x}, t) = \frac{1}{c^2}\frac{\partial}{\partial t}\int g(\mathbf{x} - \mathbf{x}', t)p_0(\mathbf{x}')d\mathbf{x}', \tag{4a}$$

where

$$g(\mathbf{x}, t) = \frac{\delta(\|\mathbf{x}\| - ct)}{4\pi\|\mathbf{x}\|}. \tag{4b}$$

When the initial pressure $p_0(\mathbf{x})$ from Eq. (2) is due to a homogeneous pressure source from an absorbing object in a non-absorbing background, it can be written as

$$p_0(\mathbf{x}) = \begin{cases} P_{\text{constant}}, & \text{if } \mathbf{x} \text{ is on the object,} \\ 0, & \text{if } \mathbf{x} \text{ is on the backgound,} \end{cases} \tag{5}$$

where P_{constant} is a constant. Accordingly, Eq. (4) can be rewritten as

$$p(\mathbf{x}, t) = P_{\text{constant}}\frac{1}{4\pi c^2}\frac{\partial}{\partial t}\frac{A(\mathbf{x}, ct)}{\|\mathbf{x}\|}, \tag{6}$$

where

$$A(\mathbf{x}, ct) = \frac{1}{P_{\text{constant}}}\int_{\|\mathbf{x}-\mathbf{x}'\|=ct} p_0(\mathbf{x}')d\mathbf{x}'. \tag{7}$$

Equation (7) represents the area of intersection between the object defined in Eq. (5) and a spherical wavefront centered at $\mathbf{x}$. For the rest of this paper, we assume $P_{\text{constant}} = 1$.

III. DERIVATION FOR THE EXACT SOLUTION OF AN FINITE-LENGTH CYLINDRICAL PHOTOACOUSTIC SOURCE IN TERMS OF ELLIPTIC INTEGRALS

This derivation starts by following an approach similar to by Lamarche *et al.*,[18] where the exact solution for the volume of intersection between a solid sphere and a solid infinite-length cylinder were reduced into terms of elliptic integrals for computing atomic cross-sections. In our work, the photoacoustic pressure $p(\mathbf{x}, t)$ is obtained from Eq. (6), where the surface area of intersection is used instead of the volume of intersection. We also take additional steps to account for a finite-length cylinder instead of an infinite cylinder.

In Sec. III A, the exact area of intersection of a wavefront with an infinite cylinder is derived. In Sec. III B, this is converted to photoacoustic pressure. In Sec. III C, terms resulting from the ends of the finite-length cylinder are taken into account. In Sec. III D, it is shown how calculating pressure can be performed when the finite-length cylinder is at an arbitrary position and orientation.

A. Area of intersection of a sphere and a cylinder

We start with the derivation for the exact area of intersection between a sphere and an infinitely long cylinder. The sphere corresponds to the spherical wavefront of radius $r = ct$ centered at point O as shown in Fig. 1. The axis of the cylinder as shown is centered at point B. The radius of the cylinder is indicated by R. Without loss of generality, we can consider the case where the axis of the cylinder is perpendicular to the page. The area of intersection is defined as a function $f(x, y)$ over the region S which is shaded in Fig. 1. From calculus, the surface area of a function $f(x, y)$ over any general region S is

$$\int_S \sqrt{1 + \left(\frac{\partial f}{\partial x}\right)^2 + \left(\frac{\partial f}{\partial y}\right)^2}\, dx\, dy. \tag{8}$$

From Eq. (8), the area of intersection between a spherical wavefront and an infinite-length cylinder is derived. Let b be

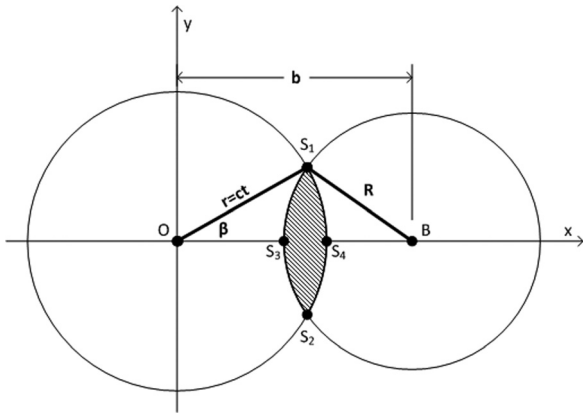

FIG. 1. Intersection of a spherical wavefront and a cylinder. The axis of the cylinder is perpendicular to the page and is centered at point B. The radius of the cylinder is R. The wavefront is centered at point O and has radius r. The region S defining where the intersection occurs is shaded.

the minimum distance from the origin O to the longitudinal axis of the cylinder B. The cylinder is defined by

$$(x-b)^2+y^2<R. \tag{9}$$

The sphere $x^2+y^2+z^2=r^2$, representing the wavefront, can be written as

$$f(x,\,y)=\pm\sqrt{r^2-x^2-y^2}. \tag{10}$$

For use in Eq. (8), the partial derivatives of Eq. (10) are

$$\begin{aligned}\frac{\partial f(x,\,y)}{\partial x}&=\mp\frac{x}{\sqrt{r^2-x^2-y^2}},\\ \frac{\partial f(x,\,y)}{\partial y}&=\mp\frac{y}{\sqrt{r^2-x^2-y^2}}.\end{aligned} \tag{11}$$

By substituting Eq. (11) into Eq. (8), the total area above and below region S is

$$\begin{aligned}A&=2\int_S\sqrt{1+\left(\frac{\partial f}{\partial x}\right)^2+\left(\frac{\partial f}{\partial y}\right)^2}\,dx\,dy\\&=2\int_S\frac{r}{\sqrt{r^2-x^2-y^2}}\,dx\,dy.\end{aligned}$$

Switching to polar coordinates with $\rho=x^2+y^2$ and $\tan\theta=y/x$, this becomes

$$A=2\int_S\frac{r}{\sqrt{r^2-\rho^2}}\rho d\rho\,d\theta. \tag{12}$$

The region S is defined in polar coordinates. As shown in Fig. 1, in the variable θ, the region S is bounded from point S_1 to point S_2, and in the variable ρ, it is bounded from S_3 to S_4. The angle at point S_1 is called β, and at S_2 the angle is $-\beta$. When $b\neq 0$, the region S has four cases as illustrated in Fig. 2, depending if $b>R$ and/or if $r>R+b$. Figure 1 is drawn according to the case shown in Fig. 2(b). As shown in Figs. 2(a) and 2(b), when $b>R$ the entire region S is bounded from $\rho=|b-R|$ to r and by $\theta=-\beta$ to β. As shown in Figs. 2(c) and 2(d), when $b-R<0$, a circular section of area is missing from the polar integration region. This missing section has the form of a fifth case for the region S where $b=0$. If $b=0$ then S is a circular region centered at the origin and A can be directly solved as

$$\begin{aligned}A(r,\,R,\,0)&=2\int_0^{2\pi}\int_0^a\frac{r}{\sqrt{r^2-\rho^2}}\rho d\rho d\theta\\&=4\pi\arcsin\left(\frac{a}{r}\right),\end{aligned} \tag{13}$$

where a is $\min(r,\,R)$. Hence, the missing area that must be accounted for when $b-R<0$ is

$$A_0=\begin{cases}0, & R\le b,\\ 4r\pi\arcsin\left(\dfrac{R-b}{r}\right), & 0<R-b<r,\\ 2\pi^2 r, & \text{otherwise.}\end{cases} \tag{14}$$

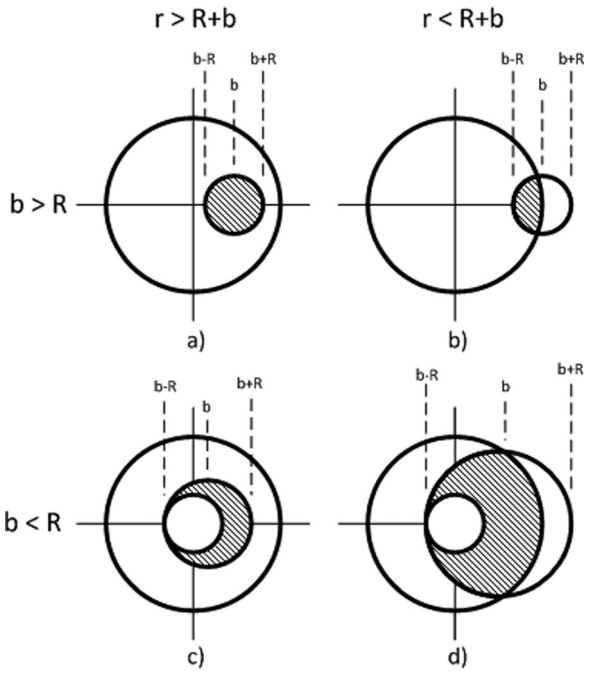

FIG. 2. Intersections of sphere and cylinder. There are four ways that a sphere of radius r can intersect an infinite cylinder of radius R. The sphere is shown centered at the origin. The distance from the center of the sphere to the axis of the cylinder is called b.

This is because the remaining portion of region S when $b-R<0$ is also bounded from $\rho=|b-R|$ to r and by $\theta=-\beta$ to β and can be solved by accounting for A_0.

Proceeding with the solution to Eq. (12), the angle β defining S can be found from the cosine law as $\beta=\arccos[(\rho^2+b^2-R^2)/2b\rho]$. By symmetry, the area is double that of the region bounded from $\theta=0$ to β. Hence, the surface area is

$$\begin{aligned}&2\int_{|b-R|}^r\int_0^\beta\frac{r\rho}{\sqrt{r^2-\rho^2}}d\theta\,d\rho\\&\quad=\int_{|b-R|}^r\frac{r\rho}{\sqrt{r^2-\rho^2}}\arccos\left(\frac{\rho^2+b^2-R^2}{2b\rho}\right)d\rho,\end{aligned} \tag{15}$$

which can be rewritten using integration by parts as A_1+A_2 where

$$A_1=-2\left[\arccos\left(\frac{\rho^2+b^2-R^2}{2b\rho}\right)r\sqrt{r^2-\rho^2}\right]_{\rho=|b-R|}^{\min(r,\,b+R)}$$

and

$$A_2=\int_{|b-R|}^{\min(r,\,b+R)}\frac{-2r\sqrt{r^2-\rho^2}\left(\rho^2-b^2+R^2\right)}{\rho\sqrt{\left(\rho^2-(R+b)^2\right)\left((R-b)^2-\rho^2\right)}}d\rho.$$

Hence, the total area of intersection above region S is

$$A=A_0+A_1+A_2. \tag{16}$$

The term A_1 reduces to

$$A_1=\begin{cases}-2\pi r\sqrt{r^2-(R-b)^2}, & 0<R-b<r,\\ 0, & \text{otherwise.}\end{cases} \tag{17}$$

To solve the term A_2, we substitute $\mu := \rho^2$ so that $d\mu = 2\rho d\rho$. Thus,

$$A_2 = \int_{(b-R)^2}^{\min\left(r^2,(b+R)^2\right)} \frac{-r\sqrt{r^2-\mu}\left(\mu - b^2 + R^2\right)}{\mu\sqrt{(\mu-(R+b)^2)((R-b)^2-\mu)}} d\mu.$$

Defining $k_1 := b^2 - R^2$, $k_2 := (b-R)^2$ and $k_3 := (b+R)^2$ this becomes

$$A_2 = 2\int_{k_2}^{\min\left(r^2,k_3\right)} \frac{(\mu - k_1)\sqrt{r^2(r^2-\mu)}}{\mu\sqrt{(\mu-k_2)(k_3-\mu)}} d\mu. \tag{18}$$

A_2 can now be solved by using the tabulated formulas for elliptic integrals[21] or with the help of a symbolic math toolbox (we used Maple[22]) as

$$A_2 = \begin{cases} 0, & r \le |b-R|, \\ \dfrac{2r(k_1+r^2-k_3)}{\sqrt{k_3-k_2}} \boldsymbol{K}\left(\sqrt{\dfrac{k_2-r^2}{k_2-k_3}}\right) \\ -\dfrac{2r(k_2-k_3)}{\sqrt{k_3-k_2}} \boldsymbol{E}\left(\sqrt{\dfrac{r^2-k_2}{k_3-k_2}}\right) \\ -\dfrac{2k_1 r^3}{k_2\sqrt{k_3-k_2}} \boldsymbol{\Pi}\left(\dfrac{k_2-r^2}{k_2}, \sqrt{\dfrac{r^2-k_2}{k_3-k_2}}\right), \\ \qquad |b-R| < r \text{ and } r \le R+b, \\ \dfrac{2rk_1}{\sqrt{r^2-k_2}} \boldsymbol{K}\left(\sqrt{\dfrac{k_3-k_2}{r^2-k_2}}\right) - \dfrac{2r(k_2-r^2)}{\sqrt{r^2-k_2}} \boldsymbol{E}\left(\sqrt{\dfrac{k_3-k_2}{r^2-k_2}}\right) \\ -\dfrac{2r^3k_1}{k_2\sqrt{r^2-k_2}} \boldsymbol{\Pi}\left(\dfrac{k_2-k_3}{k_2}, \sqrt{\dfrac{k_3-k_2}{r^2-k_2}}\right), \\ \qquad \text{otherwise.} \end{cases}$$

The functions $\boldsymbol{K}(\kappa)$, $\boldsymbol{E}(\kappa)$, and $\boldsymbol{\Pi}(\nu, \kappa)$ are the complete elliptic integrals of the first, second and third kinds in Legendre canonical form. They are defined from their respective incomplete elliptic integrals $\boldsymbol{F}(z, \kappa)$, $\boldsymbol{E}(z, \kappa)$, and $\boldsymbol{\Pi}(z, \nu, \kappa)$ by

$$\boldsymbol{K}(\kappa) = \boldsymbol{F}(1, \kappa), \quad \boldsymbol{F}(z, \kappa) = \int_0^z \frac{1}{\sqrt{1-\tau^2}\sqrt{1-\kappa^2\tau^2}} d\tau,$$

$$\boldsymbol{E}(\kappa) = \boldsymbol{E}(1, \kappa), \quad \boldsymbol{E}(z, \kappa) = \int_0^z \frac{\sqrt{1-\kappa^2\tau^2}}{\sqrt{1-\tau^2}} d\tau,$$

$$\boldsymbol{\Pi}(\nu, \kappa) = \boldsymbol{\Pi}(1, \nu, \kappa),$$

$$\boldsymbol{\Pi}(z, \nu, \kappa) = \int_0^z \frac{1}{(1-\nu\tau^2)\sqrt{1-\tau^2}\sqrt{1-\kappa^2\tau^2}} d\tau.$$

B. Photoacoustic pressure from an infinite cylinder

Using Eqs. (6) and (16), the photoacoustic pressure for the infinite cylinder can be written as

$$P = \frac{1}{4\pi c^2}\frac{\partial}{\partial t}\left[\frac{A}{r}\right]_{r=ct}. \tag{19}$$

Substituting Eq. (16) into Eq. (19), we find

$$\begin{aligned} P &= \frac{1}{4\pi c^2}\frac{\partial}{\partial t}\left[\frac{A_0 + A_1 + A_2}{r}\right]_{r=ct} \\ &= P_0 + P_1 + P_2, \end{aligned} \tag{20}$$

where

$$P_0 = \begin{cases} \dfrac{\sqrt{k_2}}{c^2 t\sqrt{c^2t^2-k_2}}, & 0 < R-b < ct, \\ 0, & \text{otherwise}, \end{cases}$$

$$P_1 = \begin{cases} -\dfrac{t}{2\sqrt{c^2t^2-k_2}}, & 0 < R-b < ct, \\ 0, & \text{otherwise}, \end{cases}$$

$$P_2 = \begin{cases} 0, & ct \le |R-b|, \\ \dfrac{t}{2\pi\sqrt{c^2t^2-k_2}}\left(\boldsymbol{K}\left(\sqrt{\dfrac{c^2t^2-k_2}{k_3-k_2}}\right)\right. \\ \left. -\dfrac{k_1}{k_2}\boldsymbol{\Pi}\left(\dfrac{k_2-k_3}{k_2}, \sqrt{\dfrac{c^2t^2-k_2}{k_3-k_2}}\right)\right), \\ \qquad |b-R| \le ct \text{ and, } ct \le R+b, \\ \dfrac{t}{2\pi\sqrt{k_2-k_3}}\left(\boldsymbol{K}\left(\sqrt{\dfrac{c^2t^2-k_2}{k_3-k_2}}\right)\right. \\ \left. -\dfrac{k_1}{k_2}\boldsymbol{\Pi}\left(\dfrac{k_2-c^2t^2}{k_2}, \sqrt{\dfrac{c^2t^2-k_2}{k_3-k_2}}\right)\right), \text{ otherwise.} \end{cases}$$

What has been presented so far in Eq. (20) is an alternate derivation for the known exact solution of an infinite-length cylindrical photoacoustic source.[7–10] However when the cylinder is finite-length, then region S is no longer the same as in Eq. (15). In Sec. III C, we describe how to account for the finite-length case.

C. Photoacoustic pressure from a finite-length cylinder

To find the exact area (or pressure), an excess amount Δ_A (or Δ_P) must be subtracted from the infinite-length case of Eq. (20) to account for the ends of the cylinder. The geometry is shown in Figs. 3 and 4 where h_1 and h_2 indicate the start and end positions of the cylinder on its coordinate axis. The exact area $A_{\text{exact}}(r, R, b, h_1, h_2)$ and pressure $P_{\text{exact}}(t, R, b, h_1, h_2)$ are

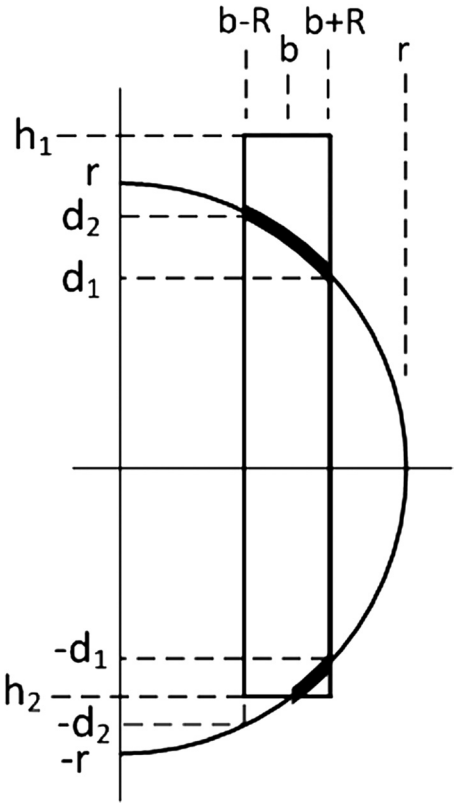

FIG. 3. Surface area of sphere-cylinder intersection; h_1 and h_2 define the start and end of the cylinder at a position on its axis; d_1 and d_2 are the positions on the cylinder axis that the sphere intersects.

$$A_{\text{exact}} = A - \Delta_A(h_1) - \Delta_A(-h_2), \tag{21a}$$

$$P_{\text{exact}} = P - \Delta_P(h_1) - \Delta_P(-h_2), \tag{21b}$$

where

$$\Delta_A(h) = \begin{cases} 0, & d_2 \le h, \\ A^*, & d_1 < h < d_2, \\ \dfrac{A}{2}, & -d_1 \le h \le d_1, \\ \dfrac{A}{2} - A^*, & -d_2 \le h \le -d_1, \\ A, & h \le -d_2, \end{cases}$$

$$\Delta_P(h) = \begin{cases} 0, & d_2 \le h, \\ P^*, & d_1 < h < d_2, \\ \dfrac{P}{2}, & -d_1 \le h \le d_1, \\ \dfrac{P}{2} - P^*, & -d_2 \le h \le -d_1, \\ P, & h \le -d_2, \end{cases}$$

and

$$A^* = A_0^* + A_1^* + A_2^*,$$
$$P^* = P_0^* + P_1^* + P_2^*,$$

with $d_1 = \max(\text{real}\{\sqrt{r^2 - (b+R)^2}\}, 0)$ and $d_2 = \min(\text{real}\{\sqrt{r^2 - (b-R)^2}\}, r)$, as shown in Fig. 3. To calculate A^* and P^*, the integration in Eq. (15) is performed from $\rho = |b-R|$ to $\sqrt{r^2 - h^2}$.

The terms A_0^*, A_1^*, and A_2^* are given by

$$A_0^* = \begin{cases} 4\pi r \arcsin\left(\dfrac{\sqrt{r^2 - h^2}}{r}\right), & 0 < R - b < \sqrt{r^2 - h^2}, \\ A_0, & \text{otherwise.} \end{cases}$$

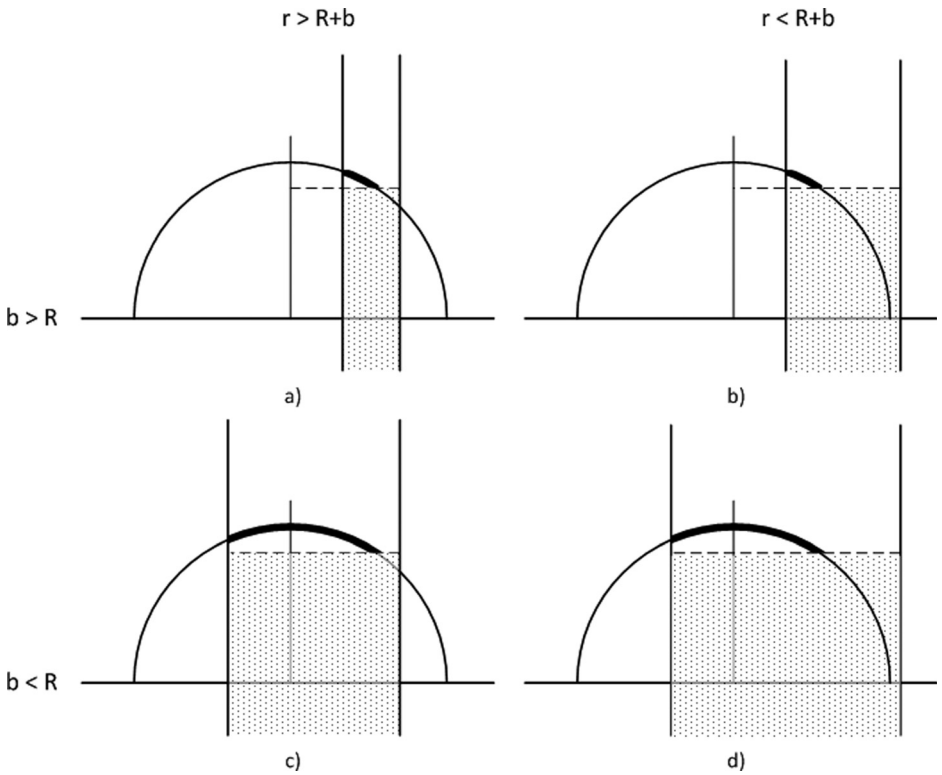

FIG. 4. The shaded surface area must be subtracted from the calculation. It must be done separately for each cylinder end. The variables are the same as in Fig. 3.

$$A_1^* = A_1 + \begin{cases} -2hr \arccos\left(\dfrac{r^2 - h^2 + k_1}{2b\sqrt{-h^2 + r^2}}\right), & |b - R| < \sqrt{r^2 - h^2}, \\ 0, & \text{otherwise.} \end{cases}$$

$$\begin{aligned} A_2^* &= 2\int_{k_2}^{r^2-h^2} \frac{(\mu - k_1)\sqrt{r^2(r^2-\mu)}}{\mu\sqrt{(\mu - k_2)(k_3 - \mu)}} d\mu \\ &= \frac{2k_1 r}{\sqrt{r^2 - k_2}} \boldsymbol{F}\left(\sqrt{\frac{r^2 - h^2 - k_2}{k_3 - k_2}}, \sqrt{\frac{k_3 - k_2}{r^2 - k_2}}\right) + \frac{2r(r^2 - k_2)}{\sqrt{r^2 - k_2}} \boldsymbol{E}\left(\sqrt{\frac{r^2 - h^2 - k_2}{k_3 - k_2}}, \sqrt{\frac{k_3 - k_2}{r^2 - k_2}}\right) \\ &\quad - \frac{2r^3 k_1}{k_2\sqrt{r^2 - k_2}} \boldsymbol{\Pi}\left(\sqrt{\frac{r^2 - h^2 - k_2}{k_3 - k_2}}, \frac{k_2 - k_3}{k_2}, \sqrt{\frac{k_3 - k_2}{r^2 - k_2}}\right). \end{aligned}$$

The terms P_0^*, P_1^*, and P_2^* are given by

$$P_0^* = \begin{cases} \dfrac{h}{t\sqrt{c^2t^2 - h^2}c^2}, & 0 < R - b < \sqrt{c^2t^2 - h^2}, \\ P_0, & \text{otherwise.} \end{cases}$$

$$P_1^* = P_1 + \begin{cases} \dfrac{ht(h^2 - c^2t^2 + k_1)}{2\pi(h^2 - c^2t^2)} \dfrac{1}{\sqrt{(c^2t^2 - h^2 - k_3)(h^2 - c^2t^2 + k_2)}}, & |b - R| < \sqrt{c^2t^2 - h^2}, . \\ 0, & \text{otherwise.} \end{cases}$$

$$\begin{aligned} P_2^* = &\frac{t}{\sqrt{c^2t^2 - k_2}} \boldsymbol{F}\left(\sqrt{\frac{h^2 - c^2t^2 + k_2}{k_2 - k_3}}, \sqrt{\frac{k_3 - k_2}{c^2t^2 - k_2}}\right) - \frac{k_1 t}{k_2\sqrt{c^2t^2 - k_2}} \boldsymbol{\Pi}\left(\sqrt{\frac{h^2 - c^2t^2 + k_2}{k_2 - k_3}}, \frac{k_2 - k_3}{k_2}, \sqrt{\frac{k_3 - k_2}{c^2t^2 - k_2}}\right) \\ &+ \frac{ht(h^2 - c^2t^2 + k_1)}{2\pi(h^2 - c^2t^2)\sqrt{(c^2t^2 - h^2 - k_3)(h^2 - c^2t^2 + k_2)}}. \end{aligned}$$

D. Arbitrarily positioned finite cylinder

The pressure $p(\mathbf{x}, t)$ can be found for an arbitrarily positioned cylinder. If the ends of the cylinder is located at positions $\mathbf{q}_2$ and $\mathbf{q}_1$, with length $L = \|\mathbf{q}_2 - \mathbf{q}_1\|$, the start and end heights of the cylinder are[23]

$$h_1 = \begin{cases} \dfrac{|(\mathbf{q}_2 - \mathbf{q}_1)\cdot(\mathbf{q}_1 - \mathbf{x})|}{L}, & (\mathbf{q}_2 - \mathbf{q}_1)\cdot(\mathbf{q}_1 - \mathbf{x}) > L^2, \\ \dfrac{|(\mathbf{q}_2 - \mathbf{q}_1)\cdot(\mathbf{q}_2 - \mathbf{x})|}{L}, & (\mathbf{q}_2 - \mathbf{q}_1)\cdot(\mathbf{q}_1 - \mathbf{x}) < 0, \\ -\dfrac{|(\mathbf{q}_2 - \mathbf{q}_1)\cdot(\mathbf{q}_1 - \mathbf{x})|}{L}, & \text{otherwise,} \end{cases} \tag{22a}$$

and

$$h_2 = \begin{cases} \dfrac{|(\mathbf{q}_2 - \mathbf{q}_1)\cdot(\mathbf{q}_2 - \mathbf{x})|}{L}, & (\mathbf{q}_2 - \mathbf{q}_1)\cdot(\mathbf{q}_1 - \mathbf{x}) > L^2, \\ \dfrac{|(\mathbf{q}_2 - \mathbf{q}_1)\cdot(\mathbf{q}_1 - \mathbf{x})|}{L}, & (\mathbf{q}_2 - \mathbf{q}_1)\cdot(\mathbf{q}_1 - \mathbf{x}) < 0, \\ \dfrac{|(\mathbf{q}_2 - \mathbf{q}_1)\cdot(\mathbf{q}_2 - \mathbf{x})|}{L}, & \text{otherwise.} \end{cases} \tag{22b}$$

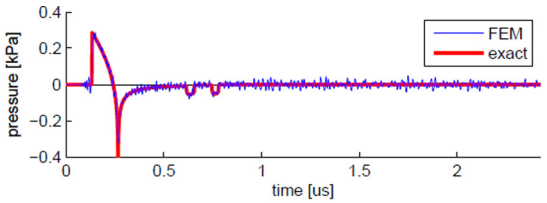

(a) FEM and Exact Solutions. $x = 0.3$mm, $y = 0.0$mm, $z = 0.1$mm

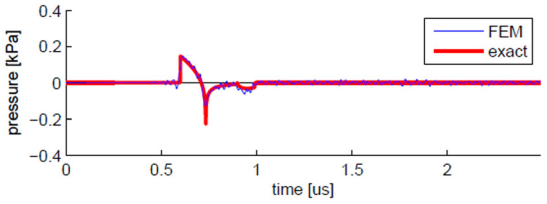

(b) FEM and Exact Solutions. $x = 1.0$mm, $y = 0.0$mm, $z = 0.0$mm

FIG. 5. (Color online) Pressure waveforms from cylindrical source. The output from the FEM solution, and the exact solution.

The distance from $\mathbf{x}$ to the cylinder axis is

$$b = \sqrt{\|\mathbf{q}_1 - \mathbf{x}\|^2 - ((\mathbf{q}_2 - \mathbf{q}_1) \cdot (\mathbf{q}_1 - \mathbf{x}))^2 / L^2}. \quad (23)$$

The exact photoacoustic pressure of the finite-length cylinder is found using Eq. (21b) as

$$p(\mathbf{x}, t) = P_{\text{exact}}(t, R, b, h_1, h_2), \quad (24)$$

where R is the radius of the cylinder, and $h_1 = h_1(\mathbf{x})$ and $h_2 = h_2(\mathbf{x})$ and $b = b(\mathbf{x})$ are defined above.

IV. FINITE ELEMENT SIMULATION

A finite element simulation is established as a reference for comparison against Eq. (24) and also to observe the acoustic wave as it propagates outward from an initial source distribution. The simulations are performed using the COMSOL[24] software package. It has a built in module for simulating acoustic wave propagation.

For our research purposes, performing a full 3D simulation on a large vascular model would not be feasible since the finite element method (FEM) requires large computational resources in terms of both memory and processing power. This is one reason why Eq. (24) was solved. Our

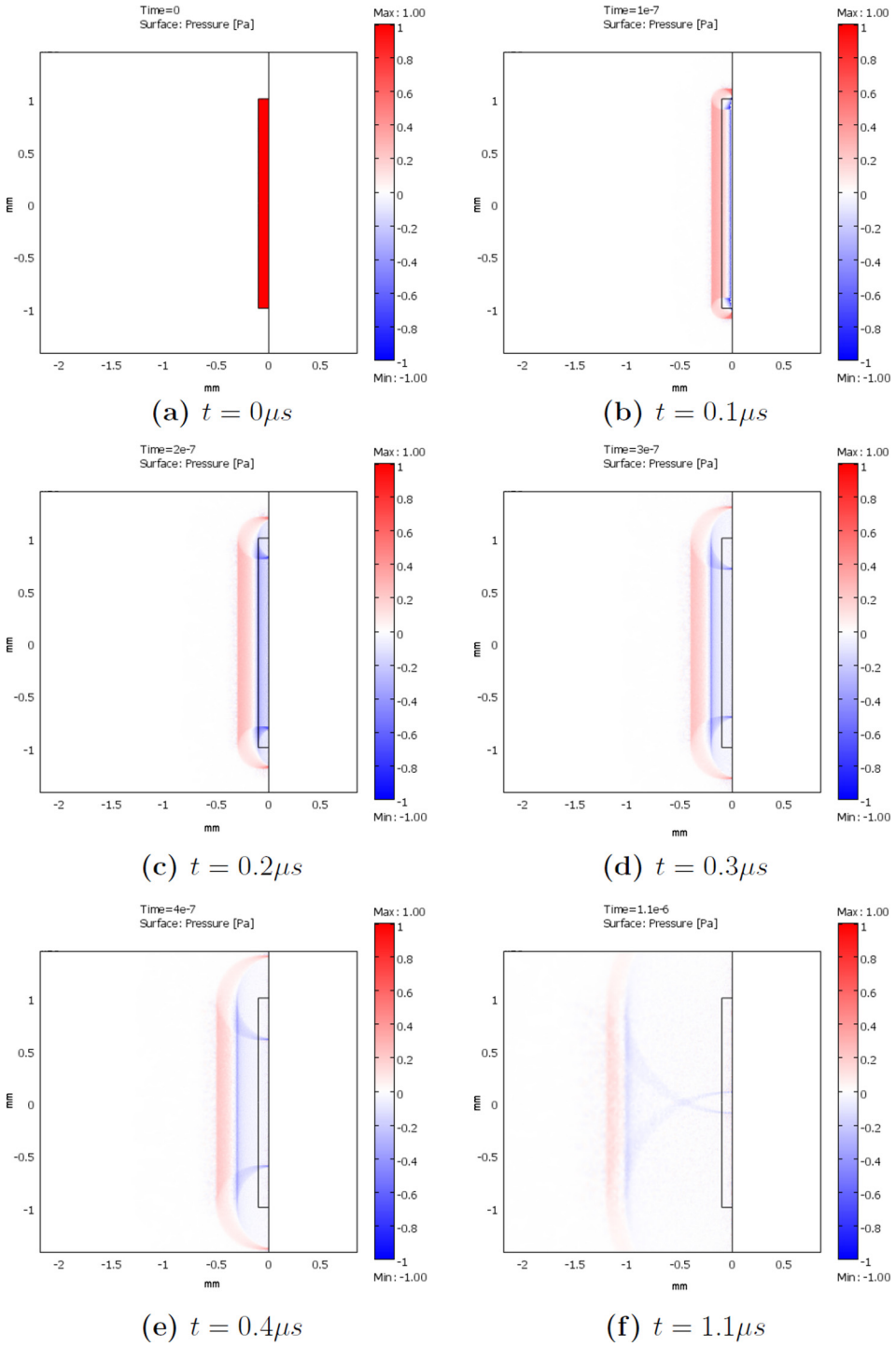

(a) $t = 0\mu s$ (b) $t = 0.1\mu s$ (c) $t = 0.2\mu s$ (d) $t = 0.3\mu s$ (e) $t = 0.4\mu s$ (f) $t = 1.1\mu s$

FIG. 6. (Color online) FEM pressure wave simulation from cylindrical photoacoustic source. $L = 2$ mm, $R = 0.1$ mm. The cylinder is centered about the vertical axis of the figure. The wavefront propagates outward in all directions with axial symmetry.

other work involves simulating a hierarchical 3D tree of cylindrical segments using a Green's function based method.[2] Software using a pseudo-spectral k-space method for simulating photo-acoustic objects of arbitrary geometry on a 3D grid could also have been used.[25] Numerical integration using Maple was also found to be in agreement with our implementation of Eq. (24). For small geometries, such as a single finite-length cylinder, the FEM is practical. In situations where there is a suitable symmetry, the 3D finite element computation can be reduced to a 2D computation. COMSOL supports a special mode for models with axial symmetry, which is the case for a cylindrical object.

The model is implemented as a 2D transient acoustic wave simulation using axial symmetry. For initial conditions, the absorbing cylinder is given an initial pressure to represent the effect of instantaneous heating immediately following the instantaneous pulse of energy deposited in the tissue. For the region inside the cylinder, the initial pressure is P_{constant} kPa. For region outside the cylinder in the background, the initial pressure is 0 kPa. The medium, both inside and outside of the cylinder, is assumed to have speed of sound 1500 m/s and density 1000 kg/m^3. The outer boundary of the simulation is given absorbing boundary conditions. The simulation is performed on a dual core 2.00 GHz Intel Pentium processor. After meshing, there were 69 572 elements and 139 727 degrees-of-freedom. The average element size was $6 \times 10^{-5}\,\text{mm}^2$ and the maximum to minimum element area ratio was 8×10^{-4}. The simulation used 489 MB of memory and completed in approximately 87 min. The results are plotted in Figs. 5 and 6. Figure 5 represents time domain waveforms for the finite element and exact solutions taken at two sampling positions. The finite element simulation is noisy and acted as a low-pass filter on the pressure signal, whereas the exact solution is noise free and the sharp negative peak of the exact solution is preserved. In Figs. 6(a)–6(f) snapshots of the wavefield at different times are shown. The simulation is axially symmetric, and the 2D slice shown can be revolved about the vertical axis of the figure corresponding to the axis of the cylinder. The wavefront shown propagates outward in all axially symmetric dimensions. The effects from the finite-cylinder ends is seen as a pressure disturbance at the tail end of the pressure signal in Fig. 5. The radiating wave propagating from the cylinder ends is seen in Fig. 6. When $z = 0.0$ mm, the effects from the ends combine into a single disturbance because the wave from each end reaches the transducer at the same time.

V. CONCLUSION

We have derived the exact solution of a photoacoustic wave resulting from the homogeneous heating of an arbitrarily positioned finite-length cylindrical source in terms of elliptic integrals. The result can take advantage of fast numerical methods for evaluating elliptic integrals in canonical form. Furthermore, this form may allow better approximations for the solution to be developed. The result has been compared against a finite element simulation and shown to be in agreement.

ACKNOWLEDGMENTS

The authors would like to acknowledge the support of an Ontario Research Fund Research Excellence (ORF-RE) grant (entitled: Focused Ultrasound Devices for Noninvasive Surgery and Drug Delivery) and the Natural Sciences and Engineering Research Council of Canada (NSERC Discovery grant) awarded to M.C.K.

[1]A. A. Oraevsky and A. A. Karabutov, *Optoacoustic Tomography* (CRC Press, Boca Raton, FL, 2003), Chap. 34, pp. 34/1–34/34.
[2]J. Zalev and M. Kolios, "Detecting abnormal vasculature from photoacoustic signals using wavelet-packet features," Proc. SPIE Photons Plus Ultrasound **7899**, 1–15 (2011).
[3]J. Zalev, "Detection and monitoring for cancer and abnormal vasculature by photoacoustic signal characterization of structural morphology," Master's thesis, Ryerson University, Toronto, Canada, 2010.
[4]R. K. Jain, "Normalization of tumor vasculature: An emerging concept in antiangiogenic therapy," Science **307**, 58–62 (2005).
[5]This means an expression consisting of a finite number of exponential, polynomial, addition, and multiplication terms.
[6]J. Remillard, "Pressure disturbances from a finite cylindrical source," J. Acoust. Soc. Am. **59**, 744–748 (1976).
[7]Y. Xu, M. Xu, and L. V. Wang, "Exact frequency-domain reconstruction for thermoacoustic tomography II: Cylindrical geometry," IEEE Trans. Med. Imag. **21**, 829–833 (2002).
[8]G. J. Diebold and T. Sun, "Properties of photoacoustic waves in one, two and three dimensions," Acustica **80**, 339–351 (1994).
[9]C. G. A. Hoelen and F. F. M. D. Mul, "A new theoretical approach to photoacoustic signal generation," J. Acoust. Soc. Am. **106**, 695–706 (1999).
[10]G. Paltauf and H. Schmidt-Kloiber, "Photoacoustic cavitation in spherical and cylindrical absorbers," Appl. Phys. A **68**, 525–531 (1999).
[11]W. X. Wang, "The exact kernel for cylindrical antenna," IEEE Trans. Antennas Propagation **39**, 434–435 (1991).
[12]D. H. Werner, "An exact formulation for the vector potential of a cylindrical antenna with uniformly distributed current and arbitrary radius," IEEE Trans. Antennas Propagation **41**, 1009–1018 (1993).
[13]P. J. Davies, B. P. Rynne, and B. Zubik-Kowal, "The time domain integral equation for a straight thin-wire antenna with the reduced kernel is not well-posed," IEEE Trans. Antennas Propagation **50**, 1165–1166 (2002).
[14]C. Wang and J. C. S. Lai, "The sound radiation efficiency of finite length acoustically think circular cylindrical shells under mechanical excitation I: Theoretical analysis," J. Sound Vib. **232**, 431–447 (2000).
[15]Z. Ye, "A novel approach to sound scattering by cylinders of finite length," J. Acoust. Soc. Am. **102**, 877–884 (1997).
[16]W. Williams, N. G. Parke, D. A. Moran, and C. H. Sherman, "Acoustic radiation from a finite cylinder," J. Acoust. Soc. Am. **36**, 2316–2322 (1964).
[17]T. K. Stanton, "Sound scattering by cylinders of finite length I: Fluid cylinders," J. Acoust. Soc. Am. **83**, 55–63 (1988).
[18]F. Lamarche and C. Leroy, "Evaluation of the volume of intersection of a sphere with a cylinder by elliptic integrals," Comput. Phys. Commun. **59**, 359–369 (1990).
[19]B. T. Cox and P. C. Beard, "Fast calculation of pulsed photoacoustic fields in fluids using k-space methods," J. Acoust. Soc. Am. **117**, 3616–3627 (2005).
[20]L. Wang, A. Bhalerao, and R. Wilson, "Analysis of retinal vasculature using a multiresolution hermite model," IEEE Trans. Med. Imaging **26**, 137–152 (2007).
[21]P. F. Byrd and M. D. Friedman, *Handbook of Elliptic Integrals for Engineers and Scientists*, 2nd ed. (Springer, New York, 1971), pp. 1–360.
[22]Maple, v13.2 (MapleSoft Inc., Waterloo, Ontario, Canada, 2009).
[23]M. Held, "ERIT—A collection of efficient and reliable intersection tests," J. Graphic Tools **2**, 25–44 (1998).
[24]COMSOL Multiphysics, v3.5a (COMSOL Inc., Burlington, MA, 2008).
[25]B. E. Treeby and B. T. Cox, "k-Wave: MATLAB toolbox for the simulation and reconstruction of photoacoustic wave fields," J. Biomed. Opt. **15**, 021314 (2010).